Solid State Ionics 300 (2017) 73–77

Contents lists available at ScienceDirect

Solid State Ionics

journal homepage: www.elsevier.com/locate/ssi

Investigation of Mg^{2+}, Sc^{3+} and Zn^{2+} doping effects on densification and ionic conductivity of low-temperature sintered $Li_7La_3Zr_2O_{12}$ garnets

Yue Jiang, Xiaohong Zhu *, Shiying Qin, Ming'en Ling, Jiliang Zhu

Department of Materials Science, Sichuan University, Chengdu 610064, China

ARTICLE INFO

Article history:
Received 15 February 2016
Received in revised form 27 October 2016
Accepted 6 December 2016
Available online xxxx

Keywords:
Solid electrolyte
$Li_7La_3Zr_2O_{12}$
Doping
Densification
Ionic conductivity

ABSTRACT

Garnet-type solid electrolytes $Li_7La_3Zr_{2-x}Mg_{2x}O_{12}$, $Li_7La_3Zr_{2-0.75x}Sc_xO_{12}$ and $Li_{7-2x}Zn_xLa_3Zr_2O_{12}$ with $x = 0$, 0.025, 0.05 and 0.1 were synthesized at 1075 °C by using the traditional solid-state reaction method. It is found that substitution of Mg^{2+} and Sc^{3+} for Zr^{4+} is more effective in improving the $Li_7La_3Zr_2O_{12}$ (LLZ)'s densification and ionic conductivity than the substitution of Zn^{2+} for Li^+. As a result, the highest room-temperature total conductivity and the lowest activation energy are obtained in LLZ-Mg-2x with $x = 0.05$, being 0.291 mS/cm at 293 K and 0.254 eV, respectively.

1. Introduction

The liquid organic electrolytes are widely used in lithium-ion batteries at present, but their flammability may cause serious safety issues; hence, inorganic solid-state electrolytes are now attracting much attention [1]. In addition, solid-state electrolytes show excellent storage stability and very long cycle life, revealing that they are highly reliable [2].

Since the first preparation of $Li_7La_3Zr_2O_{12}$ (abbreviated as LLZ) in 2007 [3], its high total conductivity, 0.24 mS/cm at 298 K, has implied that it is a promising solid electrolyte candidate to replace organic electrolytes, which is also ascribed to its high chemical stability and wide potential window. However, two phases were found to exist in LLZ, in which the conductivity of tetragonal phase is approximately two or three orders of magnitude lower than that of the cubic phase [4]. Therefore, formation and stabilization of cubic phase is an effective approach for increasing the total conductivity of LLZ [1]. Furthermore, the total conductivity of cubic phase LLZ at 298 K could be reduced to half that of the bulk conductivity because of grain boundary resistance; hence, minimizing the grain boundary resistance is also an effective approach for enhancing the total conductivity in this solid electrolyte [5].

More importantly, a dense microstructure related to the grains and grain boundaries is crucial for achieving a high total conductivity in LLZ [6]. On one hand, several sintering methods were used to get a dense microstructure, such as flowing oxygen sintering [7] and field-assisted sintering technology [8]. On the other hand, ionic doping was adopted to obtain a higher density or relative density in LLZ, such as a sole ionic doping like Al^{3+} [9], Sr^{2+} [10], Ga^{3+} [11], Ce^{4+} [12], Ta^{5+} [13], Sb^{3+} [14], Te^{4+} [15] and co-doping like Y^{3+} and Ta^{5+} [6], Al^{3+} and Te^{4+} [15], Al^{3+} and Ta^{5+} [16], Ga^{3+} and Ta^{5+} [16], Sb^{3+} and Ba^{2+} [17].

Very recently, first-principles studies by Lincoln J. Miara et al. [18] indicate that several novel dopants emerge in the LLZ material system, such as subvalent Sc^{3+} and Mg^{2+} on the Zr site and Zn^{2+} on the Li site. Aroused by this intriguing theoretical finding, we report here our experimental improvement of lithium-ion conductivity in $Li_7La_3Zr_2O_{12}$ by Mg^{2+}, Sc^{3+} and Zn^{2+} dopings. Unlike Yuki Kihira et al. [19] co-doped unsuccessfully Mg^{2+} on the La site, Mg^{2+} is substituted on the Zr site in this work based on the aforementioned theoretical work [18]. Also different from the high content of Zn^{2+} doping effect in LLZ by Yan Chen et al. [20], we demonstrate that a small amount of Zn^{2+} doping on Li site can improve the LLZ's total conductivity slightly. Furthermore, through comparison among these three dopants Mg^{2+}, Sc^{3+} and Zn^{2+}, it is concluded that the maximum room-temperature total conductivity and relative density as well as the minimum activation energy occur in LLZ-Mg-2x at $x = 0.05$.

2. Experiment

Doped LLZ compounds were prepared by the conventional solid-state reaction route. Stoichiometric quantities of $LiOH \cdot H_2O$ (Sinopharm Chemical Reagent, 95%), La_2O_3 (Sinopharm Chemical Reagent, 99.99%), ZrO_2 (Sinopharm Chemical Reagent, 99%), Sc_2O_3 (99.99%, Aldrich), ZnO (Sinopharm Chemical Reagent, 99%) and MgO (Sinopharm Chemical Reagent, 99.99%) were used as raw materials corresponding to the nominal compositions of garnet ceramics $Li_7La_3Zr_{2-x}Mg_{2x}O_{12}$,

* Corresponding author.
E-mail address: xhzhu@scu.edu.cn (X. Zhu).

http://dx.doi.org/10.1016/j.ssi.2016.12.005
0167-2738/

$Li_7La_3Zr_{2-0.75x}Sc_xO_{12}$ and $Li_{7-2x}Zn_xLa_3Zr_2O_{12}$ with $x = 0$, 0.025, 0.05, 0.1, respectively. To begin with, the starting materials were weighed out in their intended stoichiometric proportions with an excess of 10 wt% $LiOH \cdot H_2O$ to compensate for Li loss during synthesis. The powders were ball-milled with zirconia balls for about 12 h in 2-propanol in air. Then the homogenously mixed powders were calcined at 1000 °C for 12 h and cooled down to room temperature with a slow cooling rate of 1 °C/min. After ball-milled for 12 h again, the mixture was pressed under 30 MPa for 5 min into pellets of 10 mm diameter and 1 mm thickness. Finally, the pellets were sintered in air at 1075 °C for 12 h with an optimized condition. Note that all the heat treatments were conducted in alumina crucibles (>99% Al_2O_3), which were covered by alumina lids.

Powder crystalline phase identification was carried out using a DX-2700 X-ray diffractometer (XRD, Dandong, China) operated at 40 kV, 30 mA with Cu Kα radiation with the 2θ step of 0.02°. The morphologies and EDX mapping were measured by field emission-scanning electron microscopy (FE-SEM, JSM-7500, Japan). Chemical composition analysis was performed by using an inductively coupled plasma mass spectrometer (ICP-MS, Agilent 7700, USA), for which roughly 100 mg powder was collected from the sintered pellets. Archimedes' method was used to evaluate the relative density of the pellet. For electrical measurement, both faces of the pellet samples were polished and sputtered with Au to serve as electrodes, thus obtaining Au-covered LLZ pellets of about 1 mm thickness for the impedance measurements. Room-temperature conductivity measurements were performed by the impedance spectroscopy method using an Agilent 4294A precision impedance analyzer over the frequency range of 40 Hz to 110 MHz. The lithium-ion conductivities were obtained by analyzing the impedance data with Zview2 software for simulation. The activation energy of those pellets was measured by using an electrochemical workstation (CHI 660E, CH Instruments, Inc., Austin, TX, USA) loaded with a temperature control equipment from 293 to 363 K.

3. Results and discussion

The XRD patterns of LLZ-Mg, LLZ-Sc and LLZ-Zn with different doping contents after sintered at 1075 °C for 12 h are shown in Fig. 1, which matched well with the standard pattern known as cubic garnet phase $Li_5La_3Nb_2O_{12}$ (PDF 45-0109). Interestingly, one can see that the diffraction peak between 30° and 31° shifts apparently with ionic dopings. The unit-cell lattice parameter, a_0, was therefore evaluated carefully by Rietveld analysis, and the results are shown in Table 1. The lattice parameter of pure LLZ is obtained to be 13.0495 Å, which is slightly larger than that (12.9682 Å) of the cubic phase LLZ sintered at a higher temperature of 1230 °C for 36 h [3]. In the case of Mg doping, the lattice

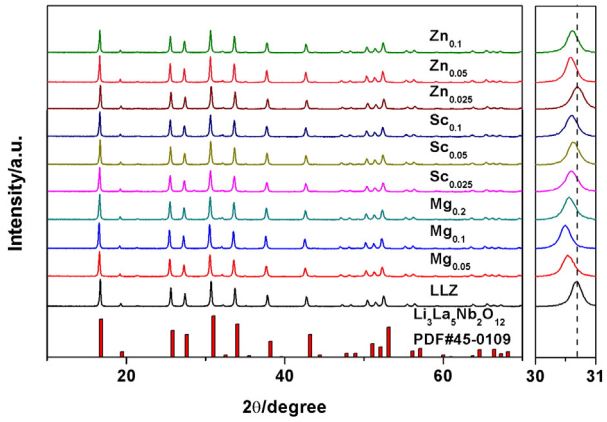

Fig. 1. (Left) XRD patterns and (Right) peak shift of $Li_7La_3Zr_{2-x}Mg_{2x}O_{12}$, $Li_7La_3Zr_{2-0.75x}Sc_xO_{12}$ and $Li_{7-2x}Zn_xLa_3Zr_2O_{12}$ with $x = 0$, 0.025, 0.05 and 0.1, sintered at 1075 °C for 12 h in the air.

Table 1
Lattice parameter (Å) of LLZ-Mg-2*x*, LLZ-Sc-*x* and LLZ-Zn-*x*.

Doping content *x*	Mg-2*x*	Sc-*x*	Zn-*x*
0.025	13.0777	13.0510	13.0473
0.05	13.0826	13.0721	13.0630
0.1	13.0798	13.0689	13.0564

Lattice parameter of pure LLZ is 13.0495 Å.

parameter increases firstly with increase of doping content until $x = 0.05$, and then decreases slightly with a further increase in the doping content. The variation of lattice parameter for Sc doping displays a similar trend. On the other hand, when the content of Zn^{2+} dopant is rather low, compared to pure LLZ, the lattice parameter is slightly decreased to 13.0473 Å. As the Zn^{2+} content is further increased, the lattice parameter increases until $x = 0.05$, but slightly decreased again at $x = 0.1$. The variation of lattice parameter in Mg^{2+} and Sc^{3+} doping cases may be explained by this reason: Mg^{2+} and Sc^{3+} ions would have priority to occupy the Zr site based on the nominal stoichiometry and the theoretical results by Miara et al. [18]. Because the subvalent Mg^{2+} and Sc^{3+} ions were introduced into the LLZ lattice in terms of charge balance, the limited Zr^{4+} sites would be shared initially by more Mg^{2+} and Sc^{3+} ions, thus leading to an enlargement of unit cell and an increased lattice parameter; however, with a further increase in doping content, the site occupation would be saturatedly performed by one Mg^{2+} or Sc^{3+} ion on one Zr^{4+} site, and because the ionic radius of Mg^{2+} (0.66 Å) and Sc^{3+} (0.73 Å) is smaller than that of Zr^{4+} (0.79 Å), the further added Mg^{2+} and Sc^{3+} dopants could lead to a decreased lattice parameter. For Zn^{2+} doping, however, the Li^+ sites were occupied by less high-valent Zn^{2+} ions in order to keep charge balance, thus resulting in an initial decrease in lattice parameter at the low doping level, and then with an increase of doping content, larger Zn^{2+} ions (0.74 Å) would substitute precisely the Li^+ (0.68 Å), thereby increasing the lattice parameter, whereas Zn^{2+} may insert into grain boundaries rather than enter the lattice when the doping content is further increased, thus making the lattice parameter almost unchanged.

The SEM images of fractured surface (cross section) of pure LLZ, LLZ-Mg, LLZ-Sc and LLZ-Zn after sintered at 1075 °C in air for 12 h are shown in Fig. 2. It is presented in the SEM images of pure LLZ (Fig. 2(a)) that the grains are not in good contact with each other, implying a low density. On the other hand, those images for LLZ-$Mg_{0.1}$ (Fig. 2(b)), LLZ-$Mg_{0.2}$ (Fig. 2(c)), LLZ-$Sc_{0.05}$ (Fig. 2(d)), LLZ-$Sc_{0.1}$ (Fig. 2(e)), LLZ-$Zn_{0.05}$ (Fig. 2(f)) and LLZ-$Zn_{0.1}$ (Fig.2(g)) exhibit a distinctively flattened morphology without any noticeable grain boundaries, regardless of what the doping content is. Nonetheless, similar to the results reported in literature for LLZ [6,21], a certain amount of pores were observed in the doped LLZ samples. In contrast, there are no pores in their surface morphologies. For example, the surface SEM image of LLZ-$Mg_{0.1}$ is given in Fig. 2(h), which illustrates a dense and homogenous microstructure. The occurrence of pores might be due to the evaporation of lithium compounds and subsequent shrinkage during grain growth [22]. And because the surface was covered with mother powder during the sintering process, the evaporation of lithium compounds can be compensated; however, the inner part cannot get compensation, so pores were formed there.

The elemental stoichiometry in the LLZ-based pellets sintered at 1075 °C is experimentally determined to be Li^+:La^{3+}:Zr^{4+} = 7:2.96:1.80 from the ICP-MS measurement, which agrees well with the nominal ratio in LLZ (7:3:2). Yutao Li et al. [23] suggested that Al_2O_3 from alumina crucible might act as a sintering aid and was located primarily in the grain boundaries. Accordingly, we believe that Al_2O_3 should locate also in the LLZ's grain boundaries in our case. However, it is noteworthy that there is no other detectable phase in all the XRD patterns for both pure and doped LLZ, as presented in Fig. 1. EDX (energy-dispersive X-ray spectroscopy) mapping was then performed on the LLZ, LLZ-$Mg_{0.1}$, LLZ-$Sc_{0.05}$ and LLZ-$Zn_{0.025}$ samples for localization of